Ion Binding Site Structure and the Role of Water in Alkaline Earth EDTA Complexes

*Madison M. Foreman and J. Mathias Weber**

JILA and Department of Chemistry, University of Colorado, 440 UCB, Boulder, CO 80309-0440, USA.

AUTHOR INFORMATION

Corresponding Author

*weberjm@jila.colorado.edu

ABSTRACT. The interactions between molecular hosts and ionic guests and their dependence on the chemical environment are challenging to disentangle from solution data alone. The vibrational spectra of cold complexes of ethylenediaminetetraacetic acid (EDTA) chelating alkaline earth dications in vacuo encode structural characteristics of these complexes and their dependence on the size of the bound ion. The correlation between metal binding geometry and the relative intensities of vibrational bands of the carboxylate groups forming the binding pocket allows us to characterize water-induced changes in molecular geometry. The evolution of these structural markers from bare ions to water adducts to aqueous solution illustrates the role of water for the structure of ion binding sites in chelators. The binding pocket of EDTA opens up in aqueous solution, bringing the bound ion closer to the mouth of the binding site, and leading to an increased exposure of the ion to the chemical environment.

TOC GRAPHICS

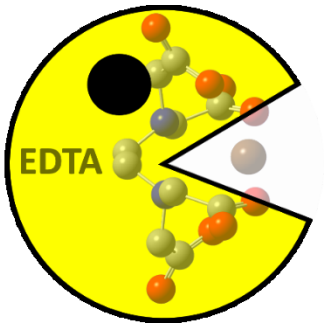

KEYWORDS. Chelates; Cryogenic Ion Vibrational Spectroscopy; Host-guest complexes; Solvation.

Supramolecular structures binding metal dications are of interest in a wide range of chemical and biological contexts, from chelators and receptors for sensing[1-2] to metal binding proteins in signal transduction and muscle action.[3-5] On a coarse scale of interactions, the properties of such binding sites are governed by the nature of the ion-coordinating ligands and the structure of their binding pockets. These pockets are often constructed by a combination of carbonyl and carboxylate functional groups that interact with the ion,[5] e.g., in many chelating agents, and in proteins such as calmodulin and other EF hand proteins.[6] On a more subtle level, the behavior of an ion binding site also depends on the chemical environment of the pocket. Apart from protein environments, water molecules play a key role in this context, since they can interact with both the metal ion and the constituents of the binding pocket, and thus have the potential to alter the interplay between the host molecule and the guest ion. In addition, the competition between ion binding and ion hydration is crucial for binding and selectivity, and this issue has been at the forefront of host-guest chemistry in recent years.[7-8]

Infrared (IR) spectroscopy has been shown to offer powerful probes for the structure and dynamics of ion binding sites.[9-10] Aminopolycarboxylic acids offer molecular models for binding pockets, with ethylenediaminetetraacetic acid (EDTA) being the most prototypical member of this group, and such models afford simplified access to the IR signatures of ion binding structures compared to the study of full proteins. However, the condensed phase environment complicates the direct connection of IR spectroscopic information even to such structural models due to the complex chemical environment of solutions.

Cryogenic ion spectroscopy methods[11-20] provide a complementary approach to uncover structural details of complex molecular systems through mass selection of spectroscopic targets in vacuo, affording a high level of control of the chemical environment, including an ability to probe

the effects of a small number of water molecules on the molecular structure of solute ions. EDTA is an archetypal and widely used chelator, with four carboxylate groups and two nitrogen atoms forming a binding pocket for cationic guests (Figure 1), and it has been used as a model system for Ca^{2+} binding pockets in EF hand proteins.[9] It binds metal ions in a hexa-coordinated fashion, forming complexes with C_2 symmetry and approximately octahedral coordination in the case of alkaline earth dications as shown in Figure 1. These complexes are accessible to cryogenic ion spectroscopy methods through electrospray ionization, and their electronic structure has been studied by photoelectron spectroscopy in this fashion.[21-23] In the present work, we use cryogenic ion vibrational spectroscopy (CIVS, see ref. [24] and Supporting Information for experimental and computational methods) to characterize the IR signatures encoding the structure of EDTA binding alkaline earth metal ions M^{2+} (M = Ca, Mg, Sr, and Ba).

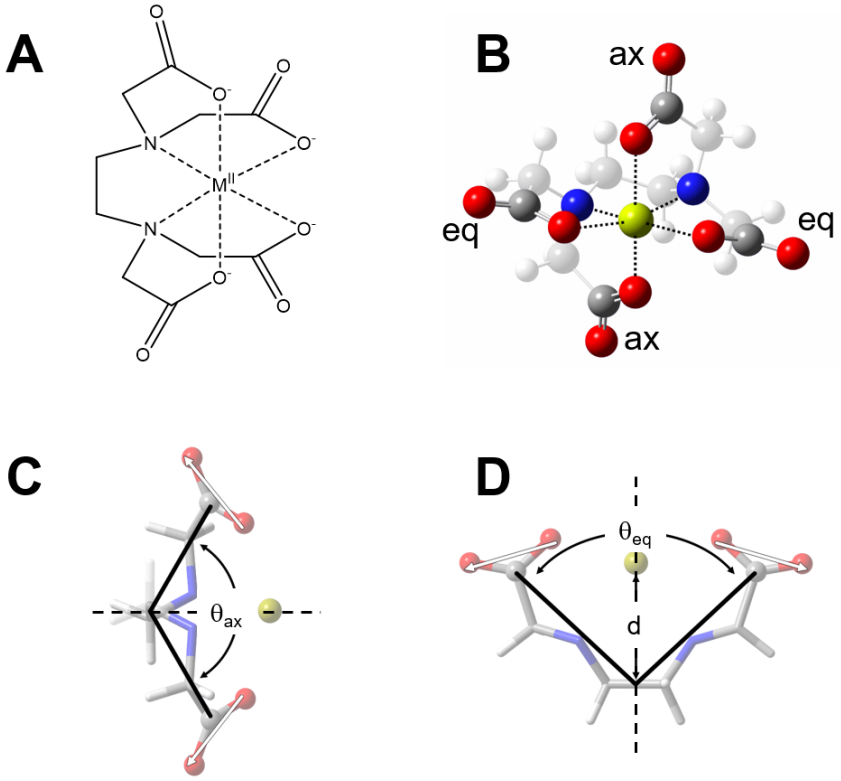

Figure 1. Geometry of EDTA complexes with alkaline earth dications. (A) $[M(II)\cdot EDTA]^{2-}$ line drawing. (B) Calculated ball-and-bond type structure of $[M(II)\cdot EDTA]^{2-}$ highlighting the binding pocket (see Supporting Information for computational details). Axial and equatorial carboxylate ligands are labeled "ax" and "eq", respectively. (C) Axial slice of $[M(II)\cdot EDTA]^{2-}$ with the definition of the axial opening angle, θ_{ax}. (D) Equatorial slice of $[M(II)\cdot EDTA]^{2-}$ with the definition of the equatorial opening angle, θ_{eq}, and the ion position, d. In parts C and D, the C_2 axis is shown as a dashed line, and light grey arrows indicate the direction of the transition dipole in each carboxylate group. Colors for the highlighted atoms: red for O, dark grey for C, blue for N, and yellow for the metal ion.

Figure 2 shows the vibrational spectra of all four complexes in the region of the antisymmetric OCO stretching vibrational bands of the carboxylate groups (full IR fingerprint region shown in Figure S1). The vibrational modes assigned to each spectral feature are identical for all four complexes, and the measured transition energies as well as a detailed assignment are given in Supporting Information (text and Table S1). The two peaks observed in each spectrum (**a** and **b**) contain four partially resolved OCO antisymmetric stretching modes[9] with patterns of motion representing different in-phase vs. out-of-phase combinations of these vibrations in all four of the EDTA carboxylate groups (see Supporting Information text and Figure S2). The highest frequency feature (**a**) corresponds to the all in-phase combination of these motions, while the most intense feature (**b**) encompasses the remaining three unresolved linear combinations of the local antisymmetric stretching motions.

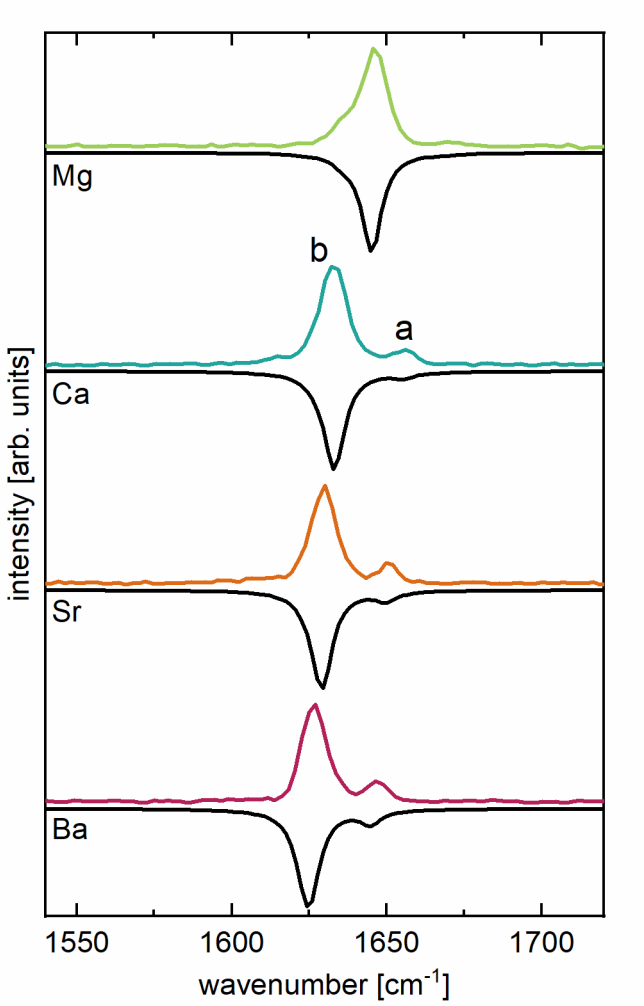

Figure 2. Comparison of experimental (upright traces) and simulated (inverted traces) spectra of $[M(II)\cdot EDTA]^{2-}$ complexes. The spectra show the region of the antisymmetric OCO stretching vibrations, with the metal indicated below each set of traces (top to bottom, Mg, Ca, Sr, Ba). Simulated IR spectra are based on scaled harmonic calculations with each mode represented by a Lorentzian line shape with 8 cm^{-1} full width at half-maximum. For a discussion of features **a** and **b** see text.

As the size of the chelated ion increases,[25] the opening angles of the binding pocket (defined in Figure 1) and the distance of the ion from the central C-C bond (ion position, *d*) increase (Figure 3). The spectroscopic features of the IR spectra encode information on the structure of each complex, allowing experimental verification of this trend in addition to the computational data. The configuration of the carboxylate groups is reflected in the relative intensity I_a of peak **a**,

defining it as $I_a = A_a / (A_a + A_b)$, where A_a and A_b are the areas under features **a** and **b**, respectively. We choose the equatorial opening angle of the binding pocket, θ_{eq}, and the ion position in the pocket, d, both defined in Figure 1, to illustrate the geometry dependence of I_a, since they present particularly clear correlations of I_a with significant geometry changes (Figure 3). Analogous data for θ_{ax} are given in Figure S4.

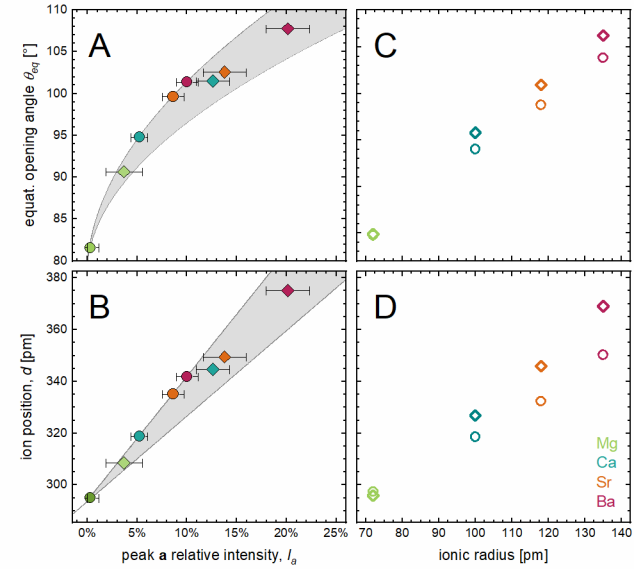

Figure 3. Correlation of the ion size and the relative intensity I_a with geometry parameters of the binding pocket. Data points are color coded for each metal as shown in panel D. (A) Equatorial opening angle and (B) ion position as defined in Figure 1, determined from the experimental relative intensity of peak a for each metal (see Figure S5 for a detailed comparison of calculated and experimental data for this model). (C) Calculated equatorial opening angle and (D) ion position as a function of ionic radius for each metal. Filled circles represent experimental data from $[M(II)\cdot EDTA]^{2-}$ complexes in vacuo. Filled diamonds show experimental data taken in aqueous solution (D_2O). In each of the two data sets, I_a increases from Mg^{2+} to Ba^{2+}. The grey shaded areas, determined by using the calculations in vacuo and with the PCM model as limiting cases, allow estimates of the geometry parameters of the EDTA binding pocket in aqueous solution. Computational data points and their comparison to the experimental values of I_a are shown in Figure S5. Error bars are $\pm 1\sigma$ uncertainties arising from a nonlinear parameter fit of the peak areas for peaks **a** and **b**.

While the nature of the ion modifies the calculated binding pocket geometry, the relative intensities of the antisymmetric OCO stretching modes in vacuo depend predominantly on the conformation of the carboxylate groups themselves (Supporting Information). This geometry dependence can be traced to the orientations of the local transition dipole moments in each carboxylate group. Choosing the C_2 symmetry axis of the complexes as the *z*-axis, the *x* and *y* components of the local OCO antisymmetric stretching transition dipoles of each equatorial and axial pair of carboxylate groups cancel for the mode giving rise to feature **a** (see Figure 1 and Supporting Information), leaving only the *z* components for generating IR activity in this mode. As larger ions displace the carboxylate groups outward, and the opening angles of the binding pocket increase, the *z* projection of the transition dipole increases as well (Figure 1), resulting in the observed growth of I_a along the sequence from Mg^{2+} to Ba^{2+}.

This direct correlation allows us to quantitatively model the binding pocket geometry by predicting the equatorial opening angle, θ_{eq}, and the ion position, *d*, from fits of the calculated geometry parameters as a function of the calculated I_a (Figure 3). The ion position scales linearly with I_a, while the equatorial opening angle can be described as $I_a \propto \sin^2\left(\frac{\theta_{eq}}{2} - \delta\right)$, where δ is a fitting parameter. Note that the linear correlation of *d* and I_a is empirical, while the behavior of θ_{eq} is based on the physical model behind I_a (see above). We use the fit functions for θ_{eq} and *d* to determine the geometry parameters in the EDTA complexes of the ions under study from the experimental values of I_a, which we obtain from each spectrum by fitting both features with Lorentzian profiles.

Both the calculated and experimental I_a values increase along the sequence from Mg^{2+} to Ba^{2+}, indicating that larger ions are bound closer to the rim of the binding pocket, and that the opening angle of the pocket increases as well. Since the ionic radius also increases along this sequence, the

trend in the geometry change is consistent with chemical intuition (Mg^{2+}, Ca^{2+}, Sr^{2+}, and Ba^{2+} have ionic radii[25] of 0.72 Å, 1.00 Å, 1.18 Å, and 1.35 Å, respectively). The correlation between ion radius and the geometry parameters shown in Figures 3.C and 3.D appears to be close to linear, but we do not infer any (predictive) model with this purely empirical trend.

In addition to the changes in relative intensity, features **a** and **b** shift to lower frequencies upon changing the ion from Mg^{2+} to Ba^{2+}, by a total of 23 cm^{-1} and 19 cm^{-1}, respectively. Different from the intensity ratio discussed above, which depends mainly on the geometry of the binding pocket (see Supporting Information text and Figure S7), the observed frequency shifts are caused by a combination of several factors. One contribution comes from the overall difference in complex geometry. The difference in the electric field generated by the metal ion at the positions of the carboxylate groups also has an effect on the frequency position, which can be described in terms of the vibrational Stark effect. However, these two factors are not independent, since the ion identity influences both the structure and the electric field. Simulated spectra where the ion identity was varied, but the EDTA complex structure was frozen (Figure S7) show how both effects play out. A third contribution is the local asymmetry of the C-O bond lengths between the "inner" O atom coordinating the metal and the "outer", free O atom in each carboxylate group (Figs. 1.C and 1.D). This asymmetry impacts the splitting of the symmetric and antisymmetric vibrational frequency of each local carboxylate, and therefore the frequencies of the normal modes of the complex as well. As a result of the subtle interplay of multiple factors, the frequency positions of the peaks are less straightforward to use as a tool for determining the geometry of the binding pocket quantitatively, but we can qualitatively associate a lower frequency with a more open binding pocket and an ion position closer to the rim of the pocket.

The presence of solvent molecules can be expected to perturb the geometry of the binding pocket, but it is challenging to obtain computational predictions for this case. On the one hand, the simulation of a sufficient number of explicit solvent molecules can be computationally expensive to the point of being unfeasible, both regarding the total size of the system and the large number of possible solvent conformations around a solute complex as large as $[M(II)\cdot EDTA]^{2-}$. On the other hand, the use of polarizable continuum models (PCM) for solvation completely neglects the molecular structure of the solvent, which makes the predictions less reliable, particularly in the case of water, which forms hydrogen bonded solvation networks.

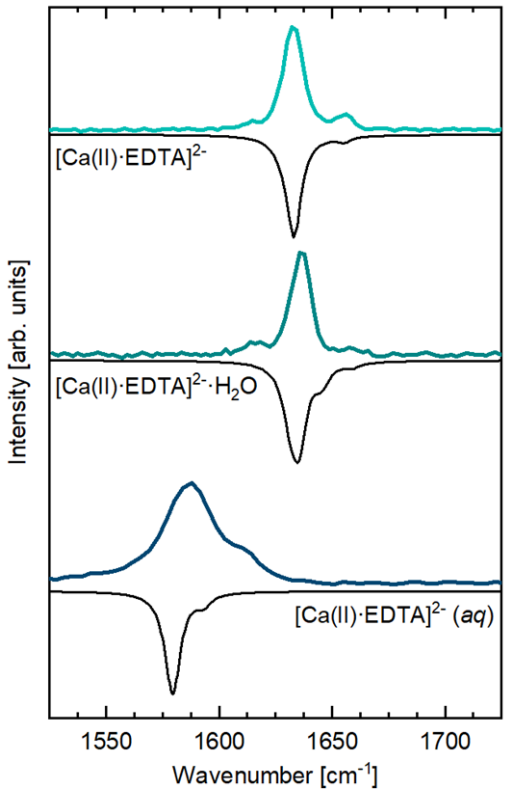

Figure 4. IR spectra of $[Ca(II)\cdot EDTA]^{2-}$ at different levels of hydration. The spectra of the bare $[Ca(II)\cdot EDTA]^{2-}$ ion (top trace) and of $[Ca(II)\cdot EDTA]^{2-}\cdot H_2O$ in vacuo (center) are compared to $[Ca(II)\cdot EDTA]^{2-}$ in D_2O solution (bottom trace).

Figure 4 shows the antisymmetric OCO stretching signatures of $[Ca(II)\cdot EDTA]^{2-}$ for the bare ion, the singly hydrated complex, and the fully hydrated complex in D_2O solution, along with computational predictions (see Figure S10 for solution phase spectra for all ions). Addition of a single water molecule leads to a weak blue shift of features **a** and **b** by 1 cm^{-1} and 5 cm^{-1}, respectively. Exploratory measurements on dihydrated $[Ca(II)\cdot EDTA]^{2-}$ show that the frequency of peak **b** is the same as for the monohydrate (Figure S9). In contrast, both features **a** and **b** show a red shift of 45 cm^{-1} upon full hydration. Interestingly, PCM calculations recover the observed red shift of feature **b** for aqueous solutions rather well (Figure 4). This implies that they capture some of the changes in the charge distribution within the carboxylate groups, which affects the force constants of the CO bonds and thereby the frequency positions of the OCO stretching vibrations. For $[Ca(II)\cdot EDTA]^{2-}$, the relative intensity of peak **a**, I_a, remains around 0.05 for the bare and singly hydrated complex, but increases to 0.13 in aqueous solution. We use the PCM calculations to construct model curves for the equatorial opening angle and ion position in analogy to the curves derived from calculations for the bare ions. We note that while the calculations for bare complexes recover the splitting between peaks **a** and **b** quite well, the PCM calculations predict a narrowing of the splitting, while the experimental splitting increases for all metals under study, leading to a deviation of the calculations by a factor of two. In addition, there is less quantitative agreement of the PCM values for I_a with aqueous solution data than for the data in vacuo. In view of these discrepancies, we judge that the accuracy of the PCM based curves in Figure 3 is lower than for the bare complexes, and we therefore treat the model curves from the two scenarios (bare ions vs. PCM) as limiting cases for the modeled pocket geometry in aqueous solution to estimate the geometric parameters for the EDTA binding pocket from the experimental values of I_a in aqueous solution (grey shaded areas in Figure 3).

Both sets of model curves, which relate I_a to the geometry of the binding pocket, predict that full hydration leads to a more open, and therefore shallower, binding pocket and a binding position of the ion closer to the rim of the pocket than in the bare complex. The opening angle increases by ca. 9º for Mg^{2+} and ca. 6º for Ba^{2+}, and full hydration brings Mg^{2+} by ca. 0.14 Å further out of the pocket, while Ba^{2+} changes its position in the pocket by ca. 0.33 Å. We qualitatively explain the dependence of the binding pocket geometry on the level of hydration with the structural evolution of the solvent environment. A search for minimum energy conformations of the monohydrated $[Ca(II)\cdot EDTA]^{2-}$ complex (Figure S8) reveals that the first water molecule forms hydrogen bonds to the carboxylate ligands, and the oxygen atom of the water molecule can interact with the dication in the pocket. Judging from the small blue shift of features **a** and **b**, the presence of the water molecule slightly tightens the pocket, but does not deform it significantly, consistent with the negligible change in I_a. In the case of full hydration, most water molecules not directly at the opening of the pocket only bind to the "outer" O atoms. Their attractive interaction with the "outer" O atoms of the carboxylate groups will exert a net force on the carboxylate groups that pulls the pocket open. This is even the case if we neglect explicit hydrogen bonding and just describe the interaction of the charge distribution of the EDTA complex with a polarizable continuum, evidenced by the success of the PCM model in qualitatively capturing the changes in ion position and opening angles. As the hydration shell grows, solvent molecules will increasingly form hydrogen bonds to the "outer" oxygen atoms of the carboxylate groups as the complex is embedded in the hydrogen bonding network of the hydration environment. This interaction increases the opening angle of the binding pocket and pulls the chelated ion closer to its rim, reflected in the increase of I_a for each complex in aqueous solution compared to the bare complex in vacuo.

The IR spectra of alkaline earth dication complexes with EDTA clearly illustrate how the ion size governs the fit of the ion in the binding pocket and the ion position within the pocket, which will change its exposure to the solvent environment. Both factors are likely to influence the competition of ion binding and ion hydration, impacting the selectivity of a given ion receptor. The comparison with solution data shows the impact of the solvation environment on the structural and binding characteristics of the binding pocket. In particular, the molecular nature of the hydrogen bonding interactions with the binding pocket needs to be taken into account to model the binding pocket geometry in the presence of solvent. This is important not only for fully solvated chelators like EDTA, but also for chemical environments that restrict solvent access, such as ion binding pockets in proteins, where only a small number of water molecules interact with the ion and its binding site, but where the presence or absence of water molecules can impact protein function.

ASSOCIATED CONTENT

Supporting Information. The following information is available free of charge: Experimental and computational methods; assignment of vibrational features; geometry model from relative intensity I_a; dependence of relative intensity I_a on ion identity; comparison of experimental and simulated spectra of $[M(II)\cdot EDTA]^{2-}$ complexes in the fingerprint region; antisymmetric OCO stretching modes of $[M(II)\cdot EDTA]^{2-}$ complexes; lower frequency range of the spectrum of $[Ba(II)\cdot EDTA]^{2-}$; correlations of equatorial opening angle and ion position with I_a; correlation of axial opening angle with the relative intensity of peak a and ionic radius for each metal; comparison of calculated geometry models from various functionals; comparison of simulated spectra resulting from swapped ion calculations for the region of the antisymmetric OCO stretching vibrations; experimental spectrum of $[Ca(II)\cdot EDTA]^{2-}\cdot H_2O$ and predicted spectra for different hydration binding sites; comparison of experimental spectra of $[Ca(II)\cdot EDTA]^{2-}$ in various stages of hydration; IR spectra of $[M(II)\cdot EDTA]^{2-}$ in D_2O; table of transition wavenumbers for observed spectral features of $[M(II)\cdot EDTA]^{2-}$ complexes; atomic coordinates of $[M(II)\cdot EDTA]^{2-}$ complexes.

The following files are available free of charge.

Supporting Information (PDF)

AUTHOR INFORMATION

Corresponding Author

*weberjm@jila.colorado.edu

Notes

The authors declare no competing financial interests.

ACKNOWLEDGMENT

We appreciate discussion with Dr. Annette H. Erbse (University of Colorado Boulder) about the role of water in protein binding pockets, and we thank Lane Terry (University of Colorado Boulder) and Dr. Jacqueline Richardson (University of Colorado Boulder) for technical assistance. JMW gratefully acknowledges support from the U. S. National Science Foundation under awards no. CHE-1764191 and PHY-1734006. This work utilized resources from the University of Colorado Boulder Research Computing Group, which is supported by the National Science Foundation (awards ACI-1532235 and ACI-1532236), the University of Colorado Boulder, and Colorado State University.

REFERENCES

(1) Vaara, M. Agents That Increase the Permeability of the Outer Membrane. *Microbiol. Rev.* **1992,** *56*, 395-411.

(2) Valeur, B.; Leray, I. Design Principles of Fluorescent Molecular Sensors for Cation Recognition. *Coord. Chem. Rev.* **2000,** *205*, 3-40.

(3) Ghosh, A.; Greenberg, M. E. Calcium Signaling in Neurons: Molecular Mechanisms and Cellular Consequences. *Science* **1995,** *268*, 239-247.

(4) Bers, D. M. Calcium Cycling and Signaling in Cardiac Myocytes. *Annu. Rev. Physiol.* **2008,** *70*, 23-49.

(5) Tang, L.; Gamal El-Din, T. M.; Payandeh, J.; Martinez, G. Q.; Heard, T. M.; Scheuer, T.; Zheng, N.; Catterall, W. A. Structural Basis for Ca^{2+} Selectivity of a Voltage-Gated Calcium Channel. *Nature* **2014,** *505*, 56-61.

(6) Gifford, J. L.; Walsh, M. P.; Vogel, H. J. Structures and Metal-Ion-Binding Properties of the Ca^{2+}-Binding Helix-Loop-Helix EF-Hand Motifs. *Biochem. J.* **2007,** *405*, 199-221.

(7) Escobar, L.; Ballester, P. Molecular Recognition in Water Using Macrocyclic Synthetic Receptors. *Chem. Rev.* **2021,** *121*, 2445-2514.

(8) Cremer, P. S.; Flood, A. H.; Gibb, B. C.; Mobley, D. L. Collaborative Routes to Clarifying the Murky Waters of Aqueous Supramolecular Chemistry. *Nature Chem.* **2018,** *10*, 8-16.

(9) Edington, S. C.; Gonzalez, A.; Middendorf, T. R.; Halling, D. B.; Aldrich, R. W.; Baiz, C. R. Coordination to Lanthanide Ions Distorts Binding Site Conformation in Calmodulin. *Proc. Natl. Acad. Sci.* **2018,** *115*, E3126-E3134.

(10) Edington, S. C.; Baiz, C. R. Vibrational Relaxation in EDTA Is Ion-Dependent. *J. Phys. Chem. A* **2018,** *122*, 6585-6592.

(11) Brümmer, M.; Kaposta, C.; Santambrogio, G.; Asmis, K. R. Formation and Photodepletion of Cluster Ion-Messenger Atom Complexes in a Cold Ion Trap: Infrared Spectroscopy of VO^+, VO_2^+, and VO_3^+. *J. Chem. Phys.* **2003,** *119*, 12700-12703.

(12) Rizzo, T. R.; Boyarkin, O. V., Cryogenic Methods for the Spectroscopy of Large, Biomolecular Ions. In *Gas-Phase IR Spectroscopy and Structure of Biological Molecules*, Rijs, A. M.; Oomens, J., Eds. 2015; Vol. 364, pp 43-97.

(13) Asmis, K. R.; Neumark, D. M. Vibrational Spectroscopy of Microhydrated Conjugate Base Anions. *Acc. Chem. Res.* **2012,** *45*, 43-52.

(14) Wolk, A. B.; Leavitt, C. M.; Garand, E.; Johnson, M. A. Cryogenic Ion Chemistry and Spectroscopy. *Acc. Chem. Res.* **2014,** *47*, 202-210.

(15) Rijs, A. M.; Oomens, J. Ir Spectroscopic Techniques to Study Isolated Biomolecules. *Topics in current chemistry* **2015,** *364*, 1-42.

(16) Niedner-Schatteburg, G., Cooperative Effects in Clusters and Oligonuclear Complexes of Transition Metals in Isolation. In *Clusters - Contemporary Insight in Structure and Bonding*, Dehnen, S., Ed. 2017; Vol. 174, pp 1-40.

(17) Wada, K.; Kida, M.; Muramatsu, S.; Ebata, T.; Inokuchi, Y. Conformation of Alkali Metal Ion-Calix[4]Arene Complexes Investigated by Ir Spectroscopy in the Gas Phase. *Phys. Chem. Chem. Phys* **2019,** *21*, 17082-17086.

(18) Hirata, K.; Mori, Y.; Ishiuchi, S. I.; Fujii, M.; Zehnacker, A. Chiral Discrimination between Tyrosine and Beta-Cyclodextrin Revealed by Cryogenic Ion Trap Infrared Spectroscopy. *Phys. Chem. Chem. Phys* **2020,** *22*, 24887-24894.

(19) Sato, E.; Hirata, K.; Lisy, J. M.; Ishiuchi, S.; Fujii, M. Rethinking Ion Transport by Ionophores: Experimental and Computational Investigation of Single Water Hydration in Valinomycin-K^+ Complexes. *J. Phys. Chem. Lett.* **2021,** *12*, 1754-1758.

(20) Wang, X. B.; Woo, H. K.; Wang, L. S. Vibrational Cooling in a Cold Ion Trap: Vibrationally Resolved Photoelectron Spectroscopy of Cold C_{60}^- Anions. *J. Chem. Phys.* **2005,** *123*, 051106.

(21) Yuan, Q. Q.; Cao, W. J.; Wang, X. B. Cryogenic and Temperature-Dependent Photoelectron Spectroscopy of Metal Complexes. *Int. Rev. Phys. Chem.* **2020,** *39*, 83-108.

(22) Yuan, Q. Q.; Kong, X. T.; Hou, G. L.; Jiang, L.; Wang, X. B. Photoelectron Spectroscopic and Computational Studies of EDTA·M(III)$^-$ Complexes (M = H_3, Al, Sc, V-Co). *Phys. Chem. Chem. Phys.* **2018,** *20*, 19458-19469.

(23) Yuan, Q. Q.; Kong, X. T.; Hou, G. L.; Jiang, L.; Wang, X. B. Electrospray Ionization Photoelectron Spectroscopy of Cryogenic EDTA·M(II)$^{2-}$ Complexes (M = Ca, V-Zn): Electronic Structures and Intrinsic Redox Properties. *Faraday Disc.* **2019,** *217*, 383-395.

(24) Xu, S.; Gozem, S.; Krylov, A. I.; Christopher, C. R.; Mathias Weber, J. Ligand Influence on the Electronic Spectra of Monocationic Copper-Bipyridine Complexes. *Phys. Chem. Chem. Phys* **2015,** *17*, 31938-31946.

(25) Lide, D. R., *CRC Handbook of Chemistry and Physics*. 86 Ed.; Taylor & Francis Group: Boca Raton, FL, 2005.

TOC GRAPHICS